World Academy of Science, Engineering and Technology
International Journal of Materials and Metallurgical Engineering
Vol:11, No:8, 2017

A Two-Phase Flow Interface Tracking Algorithm Using a Fully Coupled Pressure-Based Finite Volume Method

Shidvash Vakilipour, Scott Ormiston, Masoud Mohammadi, Rouzbeh Riazi, Kimia Amiri, Sahar Barati

***Abstract*—**Two-phase and multi-phase flows are common flow types in fluid mechanics engineering. Among the basic and applied problems of these flow types, two-phase parallel flow is the one that two immiscible fluids flow in the vicinity of each other. In this type of flow, fluid properties (e.g. density, viscosity, and temperature) are different at the two sides of the interface of the two fluids. The most challenging part of the numerical simulation of two-phase flow is to determine the location of interface accurately. In the present work, a coupled interface tracking algorithm is developed based on Arbitrary Lagrangian-Eulerian (ALE) approach using a cell-centered, pressure-based, coupled solver. To validate this algorithm, an analytical solution for fully developed two-phase flow in presence of gravity is derived, and then, the results of the numerical simulation of this flow are compared with analytical solution at various flow conditions. The results of the simulations show good accuracy of the algorithm despite using a nearly coarse and uniform grid. Temporal variations of interface profile toward the steady-state solution show that a greater difference between fluids properties (especially dynamic viscosity) will result in larger traveling waves. Gravity effect studies also show that favorable gravity will result in a reduction of heavier fluid thickness and adverse gravity leads to increasing it with respect to the zero gravity condition. However, the magnitude of variation in favorable gravity is much more than adverse gravity.

***Keywords*—**Coupled solver, gravitational force, interface tracking, Reynolds number to Froude number, two-phase flow.

I. Introduction

TWO-PHASE and multi-phase flows are of the most applied flow types in fluid engineering. These types of flows could be classified as separated and dispersed. In dispersed flows, one phase is suspended in another phase as small particles or a bulk of very small particles. Because of the huge number of particles, tracking the interface is not important in these flows. Solid particles suspended in liquids or gases (such as fluidized beds, dusty gases and mixtures), gas or liquid bubbles floated in liquids or gases (like steam boiler and sprays), and combustion of liquid or solid particles fuels in combustion chambers are all some typical of dispersed two phases flows. In separate flows, unlike the dispersed flows, there are two distinct and unmixed phases which may become suspended in the other phase based on the flow regimes or instabilities that occur in the flow field. The formation of bubbles or drops in liquid or gas is of the most important typical of this class of two-phase flows. Although one phase is surrounded by the other one in these kinds of flows (like gas bubbles suspended in liquid), the boundary between the two phases is clearly distinctive and recognizable.

Stratified, parallel two-phase, and free surface flows are the other applicable types of separated flows. In these flows, none of the phases are surrounded by the other one. Sloshing, dam-break, and falling films are some of the examples of free surface flows. In numerical modeling of free surface flows, the gas phase is not usually resolved and replaced by a proper free surface boundary condition.

Parallel two-phase flows usually occur in pipes and horizontal or inclined channels at the presence of two non-mixing fluids (usually liquid and gas). As shown in Fig. 1, internal flow in the horizontal or inclined channels is classified into seven flow regimes [1]. The stratified and wavy regimes are both amenable to the interface-tracking approach used in this paper. The other flow regimes are often simulated using mixture model, Eulerian model, and Lagrangian Dispersed Phase Model (LDPM) approaches.

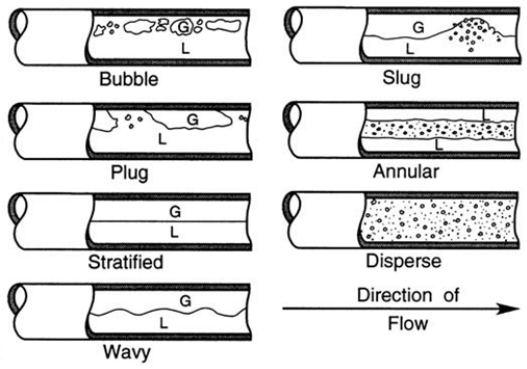

Fig. 1 Sketches of flow regimes for flow of air/water mixtures in a horizontal pipe [1]

Estimating the exact location of interface is one of the main challenges in numerical simulation of non-mixing two-phase flows. Due to the existence of moving boundary, these flows

Shidvash Vakilipour is with the Department of Aerospace Engineering, Faculty of New Sciences and Technologies, University of Tehran, Tehran, Iran (phone: 989121326951, e-mail: vakilipour@ut.ac.ir).

Scott Ormiston is with the Department of Mechanical Engineering, University of Manitoba, Manitoba, Canada R3T 5V6, (e-mail: scott.ormiston@umanitoba.ca).

Masoud Mohammadi, Rouzbeh Riazi is with the Department of Aerospace Engineering, Faculty of New Sciences and Technologies, University of Tehran, Tehran, Iran (e-mail: mas.mohammadi@ut.ac.ir, ro_riazi@ut.ac.ir).

Kimia Amiri is with the Department of Chemical Engineering, University of Amirkabir, Tehran, Iran (e-mail: kimkimamiri@gmail.com).

Sahar Barati is with the Islamic Azadi University, Tehran, Iran (e-mail: saharbarati29@gmail.com).

are ranked as hard problems in Computational Fluid Dynamics (CFD). In these problems, the location of the moving boundary must be predicted from other flow conditions through the numerical solution procedure [2].

A. Classification of Solution Approaches in Separated Two-Phase and Multi-Phase Flows

From one point of view, the methods that have been developed for defining the location of the interface can be classified as interface-tracking and interface-capturing. In interface tracking methods, the interface is assumed as a very thin layer that its position coincides on the cells surfaces. During the solution, the location of this thin surface is tracked and its coincidence on the cell faces is kept by grid movement. In interface capturing methods, the interface is not a thin surface and hence the importance of the interface coincidence with the field cells faces disappears. In these methods, interface location is defined using the estimation of volume fraction of the neighbor cells.

From another point of view, interface tracking and capturing methods are classified, with respect to the type of the governing equations and computational grid structure, into Eulerian, Lagrangian, and Eulerian-Lagrangian approaches [3]. In Eulerian methods, the coordinate system is stationary or has a constant velocity whereas the fluid velocity is independent of that. Most of the Eulerian methods use a fixed grid structure and so its cells boundaries do not coincide with the interface. Therefore, these methods do not determine the exact position of the interface. Interface-capturing methods mostly belong to the Eulerian approach. The Marker-And-Cell (MAC) method [4], which uses marker particles to define each phase and the Volume-Of-Fluid (VOF) method [5], which uses a marker function, are two of the most well-known interface-capturing methods. The main difficulty in using Eulerian methods is the difficulty of keeping the sharp boundaries of different fluid flows and the computation of the surface tension. Through this, using techniques to include the surface tension [6], sub-cells to improve the resolution of the interface [7] and level sets to mark the fluid interface [8] were introduced to obtain a more accurate result and a higher applicability of these approaches. A review of the VOF methods can be found in [9], [10].

Although the Eulerian methods are mostly capturing (not tracking) approaches, there are several moving mesh matching methods that move the computational grid in an order that is always coincident on one of the boundary cell surface [11]. These methods may be limited to the problems that do not have large deformation of interface within the computational field [12].

In Lagrangian methods, the coordinate system and fluid move with the same velocities. Thus, every computational cell holds a constant fluid amount in itself. In these methods, some errors may occur due to the unusual shape of the field cells. Intensive efforts like re-generating the mesh or re-zoning the computational field have been made to prevent these errors. Interface-capturing methods often use Lagrangian methods. Some examples of these methods can be seen in disruption of a droplet [13], investigating the initial deformation of a suspended water [14], simulating of the two-dimensional unsteady movement of some particles [15]-[17], and axisymmetric calculations of the collision of a droplet to a wall [18].

Lagrangian methods that use re-zoning techniques are also called ALE methods. These hybrid methods can usually include the advantages of both Eulerian and Lagrangian methods. Front tracking methods that were developed by Glimm et al. [19] are in the group of Eularian-Lagrangian methods. In these methods, the boundary of the two phases is marked by a separate front. However, a constant mesh that is only modified near the front is used for the fluid of each phase.

A hybrid method has been developed by Unverdi and Tryggvason [20] using front tracking and front capturing methods. They used a simple fixed mesh for the fluid flow and a separate fine mesh to track the interface. The details of this method can be seen in [21]. Interface capturing methods have the capability to be used in numerical modeling of any type of two or multi-phase flows; but as was previously mentioned, the definition of the exact interface location and calculation of parameters like shear stresses, heat, and mass transfer would be too complicated. Hassaninejadafarahani and Ormiston [22] have investigated steam condensation in a vertical pipe using an interface tracking method. They applied a mass equilibrium correction in each column of control volumes in the liquid regime to determine the interface location. Islam et al. [23] studied the kinetic energy and surface energy of a wavy liquid film flow by implementing an interface tracking method using a finite difference scheme. They observed that, in most cases, periodic disturbances superimposed at the inflow boundary grow to fully developed waves, which retain the given periodic behavior. In some cases, however, random waves appear after the fully developed waves.

B. Targets and Innovations of the Current Paper

The following assumptions are made regarding the channel two-phase flow:

1. The main derivation force of the flow is pressure gradient;
2. The inclination angle of the channel may be positive or negative to cause a favorable or adverse gravitational force, respectively;
3. The interface is continuous.
4. Shear stress is significant at the interface,
5. The interface will be sharply defined.

An interface tracking method that uses a moving mesh that follow the interface boundary is appropriate for flows involving thin liquid films. In the present study, a pressure based cell-centered finite volume method is used for numerical simulation of incompressible two-phase flow inside a two-dimensional channel. The pressure and velocity fields are coupled by a Pressure-Weighted Interpolation Method (PWIM) [27] and the discretized continuity and momentum equations are simultaneously solved. The flow equations of two phases are linked by the equations developed for the boundary surface points at the two sides of the interface. The

interface equations are implicitly discretized in terms of pressure and velocity variables. This leads to strong coupling between of the discretized equations of two phases.

In order to show the capability of the current algorithm, numerical modeling of a two-phase flow inside a 2D channel is conducted. The numerical results are validated by comparison with analytical solution that is developed in this work. In addition, the effects of changing the ratios of the properties of the two fluids are examined.

II. Analytical Solution of Two-Phase Flow with Gravitational Force

A brief description of the analytical solution of fully developed two-phase flow without a gravitational force is presented in [24]. To evaluate the applicability of the present algorithm in different flow conditions, it is necessary to present a general analytical solution for fully developed parallel two-phase flows with gravitational force. Fig. 2 shows the two-dimensional two-phase flow through a 2D channel under the effects of pressure gradient of dp/dx and gravitational acceleration g. Assuming H to be the channel height, and y=0 as the location of interface, location of upper and lower walls will be determined as $y=(1-f)H$ and $y=-fH$, respectively. Here, f is the thickness ratio of the phase 1 to the channel height. The densities, dynamic viscosities, and volumetric flow rates of the two phases are denoted by ρ_1, ρ_2, μ_1, μ_2 and Q_1, Q_2, respectively.

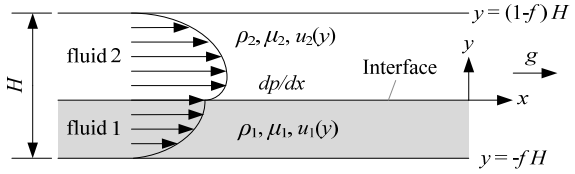

Fig. 2 The domain of a two-phase flow in a 2-D channel

Generally, the fully developed region of the flow for each of the phases shown in Fig. 2 can be assumed as a type of Poiseuille flow where, the Navier-Stokes equations are simplified to:

$$\frac{d^2u}{dy^2} = \frac{1}{\mu}\frac{dp}{dx} \tag{1}$$

This equation is written for the both phases 1 and 2. To apply the effect of gravitational force, the body force term (ρg) must be added to the equations as below:

$$\frac{d^2u_1}{dy^2} = \frac{1}{\mu_1}\left(\frac{dp}{dx} - \rho_1 g\right) \quad , \quad \frac{d^2u_2}{dy^2} = \frac{1}{\mu_2}\left(\frac{dp}{dx} - \rho_2 g\right) \tag{2}$$

To solve these equations, it is appropriate to use the non-dimension form of the equation. The non-dimensional form of the velocity, pressure and lengths are defined as:

$$u' = \frac{u}{Q_1/H}, p' = \frac{p}{\rho_1(Q_1/H)^2}, y' = \frac{y}{H}, x' = \frac{x}{H} \tag{3}$$

Using these non-dimensional parameters, (2) change to:

$$\frac{d^2u'_1}{dy'^2} = \mathrm{Re}_1\left(\frac{dp'}{dx'} - \frac{1}{f^3\mathrm{Fr}_1}\right), \quad \frac{d^2u'_2}{dy'^2} = f_\mu\mathrm{Re}_1\left(\frac{dp'}{dx'} - \frac{1}{f^3 f_\rho \mathrm{Fr}_1}\right) \tag{4}$$

where f represents the non-dimensional thickness of phase 1, $\mathrm{Re}_1 = \rho_1 Q_1/\mu_1$ is the Reynolds number of phase 1, $\mathrm{Fr}_1 = (Q_1/fH)/g(fH)$ is the Froude number of phase 1 and $f_\mu = \mu_1/\mu_2$ is the viscosity ratio of the two phases.

A. Boundary Conditions

In two-phase flows, there are three types of boundary conditions and two other conditions related to the volumetric flow rates of two phases. Their non-dimensional forms of these flows are written as follows:

– The continuity of the tangential velocity at the interface:

$$u'_1|_{y'=0} = u'_2|_{y'=0} \tag{5}$$

– The equality of the shear stress at both side of the interface:

$$\mu_1 \frac{du'_1}{dy'}\Big|_{y'=0} = \mu_2 \frac{du'_2}{dy'}\Big|_{y'=0} \tag{6}$$

- The no-slip boundary condition on the walls:

$$u'_1|_{y'=-f} = u'_2|_{y'=(1-f)} = 0 \tag{7}$$

– The known value of volumetric flow rate of the two phases:

$$1 = \int_{-f}^{0} u'_1 dy' \quad , \quad \frac{1}{f_Q} = \int_0^{1-f} u'_2 dy' \tag{8}$$

Here, $f_Q = Q_1/Q_2$ is the ratio of the volumetric flow rate of the two phases.

B. Solving the Equations

By integrating (4) and applying the boundary conditions, the velocity equations for the phases 1 and 2 are determined as:

$$u'_1 = \frac{1}{2}\mathrm{Re}_1\left(\frac{dp'}{dx'} - \frac{1}{f^3\mathrm{Fr}_1}\right)y'^2 + C_1 y' + D_1 \tag{9a}$$

$$u'_2 = \frac{f_\mu}{2}\mathrm{Re}_1\left(\frac{dp'}{dx'} - \frac{1}{f^3 f_\rho \mathrm{Fr}_1}\right)y'^2 + f_\mu C_1 y' + D_1 \tag{9b}$$

Constants C_1 and D_1 are integration constants and defined as:

$$C_1 = \frac{1}{2}\mathrm{Re}_1\left(\frac{dp'}{dx'}C - \frac{1}{f^3\mathrm{Fr}_1}C'\right) \tag{10a}$$

$$D_1 = \frac{f_\mu}{2}\mathrm{Re}_1\left(-\frac{dp'}{dx'}D + \frac{1}{f^3\mathrm{Fr}_1}D'\right) \tag{10b}$$

where,

$$C = \frac{f^2 - f_\mu(1-f)^2}{f + f_\mu(1-f)}, \quad C' = \frac{f^2 - \frac{f_\mu}{f_\rho}(1-f)^2}{f + f_\mu(1-f)} \tag{11a}$$

$$D = \frac{f(1-f)}{f+f_\mu(1-f)},\ D' = \frac{f^2(1-f)+\frac{f}{f_\rho}(1-f)^2}{f+f_\mu(1-f)} \quad (11b)$$

By substituting velocity equations (9) into volumetric flow rate equations (8) and integrating the resultant equation, the pressure gradient can be removed from the equations and the following equation is obtained:

$$f_Q = \frac{(E_1/E_2)/f_\mu}{1+\frac{\mathrm{Re}_1}{f^3\mathrm{Fr}_1}\left(F_1-\frac{E_1}{E_2}F_2\right)} \quad (12)$$

where,

$$E_1 = \frac{1}{6}f^3 - \frac{1}{4}Cf^2 - \frac{1}{2}f_\mu Df \quad (13a)$$

$$F_1 = \frac{1}{6}f^3 - \frac{1}{4}C'f^2 - \frac{1}{2}f_\mu D'f \quad (13b)$$

$$E_2 = \frac{1}{6}(1-f)^3 + \frac{1}{4}C(1-f)^2 - \frac{1}{2}f_\mu D(1-f) \quad (13c)$$

$$F_2 = \frac{1}{6f_\rho}(1-f)^3 + \frac{1}{4}C'(1-f)^2 - \frac{1}{2}f_\mu D'(1-f) \quad (13d)$$

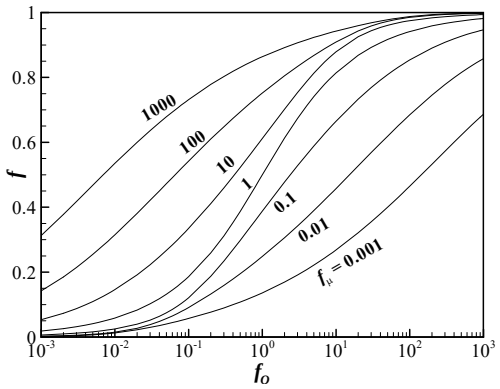

Fig. 3 Interface location (*f*) variations versus volume flow rates (f_Q) at various dynamic viscosity ratios without gravitational force

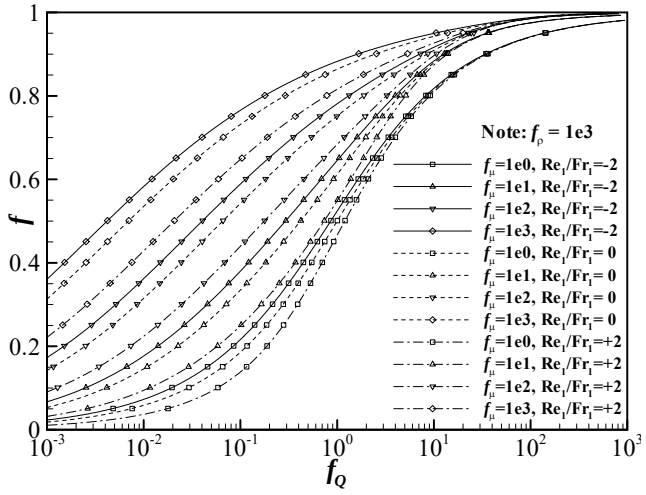

Fig. 4 Interface location (*f*) variations versus volume flow rates (f_Q) at various f_μ and $\mathrm{Re}_1/\mathrm{Fr}_1$ with gravitational force

Equation (12) is based on five known non-dimensional parameters, f, f_Q, f_μ, f_ρ, and $\mathrm{Re}_1/\mathrm{Fr}_1$, which can be solved for the unknown parameter f.

Fig. 3 shows the variations of f versus f_Q at different viscosity ratios and zero gravitational force, and Fig. 4 shows the variation of f versus other parameters at density ratio of 1000.

III. The Governing Equations and Numerical Method

A. The Governing Equations

The integral form of the governing equations of incompressible flow without source terms in a moving mesh is written as bellow:

The continuity equation

$$\frac{d}{dt}\int_\Omega \rho d\Omega + \int_S \rho(\mathbf{v}-\mathbf{v}_b)\cdot\mathbf{n}dS = 0 \quad (14)$$

The momentum equation in *x*-direction

$$\frac{d}{dt}\int_\Omega \rho U d\Omega + \int_S \rho U(\mathbf{v}-\mathbf{v}_b)\cdot\mathbf{n}dS = -\int_\Omega \frac{\partial p}{\partial x}d\Omega + \int_\Omega\left[\frac{\partial}{\partial x}\left(\mu\frac{\partial U}{\partial x}\right)+\frac{\partial}{\partial y}\left(\mu\frac{\partial U}{\partial y}\right)\right]d\Omega \quad (15)$$

The momentum equation in *y*-direction

$$\frac{d}{dt}\int_\Omega \rho V d\Omega + \int_S \rho V(\mathbf{v}-\mathbf{v}_b)\cdot\mathbf{n}dS = -\int_\Omega \frac{\partial p}{\partial y}d\Omega + \int_\Omega\left[\frac{\partial}{\partial x}\left(\mu\frac{\partial V}{\partial x}\right)+\frac{\partial}{\partial y}\left(\mu\frac{\partial V}{\partial y}\right)\right]d\Omega \quad (16)$$

where, $\mathbf{v}_b$ is the velocity of control volume boundary.

Assuring the mass conservation in discrete form of continuity equation is one of the significant challenges for moving mesh algorithm. To satisfy the mass conservation, a Space Conservation Law (SCL), is used [25]:

$$\frac{d}{dt}\int_\Omega d\Omega - \int_S(\mathbf{v}_b\cdot\mathbf{n})dS = 0 \quad (17)$$

This equation is the same as the continuity equation for zero-velocity flow.

B. Discretization of the Equations and Coupling of the Velocity and Pressure Fields

In this research, the ALE approach is used to simulate the flow in moving meshes. It can be shown that if the Lagrangian term in continuity equation is substituted with swept surface of the cell at a time step, it is not required to add the SCL equation. Therefore, for an incompressible flow, the discrete form of the Lagrangian-Eulerian equation of continuity changes to the familiar form of discrete Eulerian equation [12], [25]. This approach of discretizing the Lagrangian terms by the finite volume method leads to a formulation which does not affect the pressure-velocity coupling method.

For discretizing the momentum equation, a first-order method is used for temporal terms, and a second order method is used for pressure and shear stress terms. To estimate the convected velocities in momentum equations, the method of Exponential Differencing Scheme (EDS) is used. The

pressure-velocity fields coupling is achieved by using a PWIM similar to the approach used by Rhie and Chow [26]. These equations are discretized on a co-located grid arrangement and solved in a coupled manner. The details of this methodology can be found in the work of Vakilipour and Ormiston [27].

IV. The Boundary Conditions

There are two groups of boundary conditions implemented for the present flow computations. The inlet, outlet, and walls are considered as the first group of boundary conditions. The second group of boundary conditions includes interface boundary conditions, which are the equations governing the zero mass transfer across the interface and normal and tangential forces balance on the interface cell faces.

A. Inlet, Outlet and Wall Boundary Conditions

At the inlet section, a velocity profile is prescribed, and the pressure is extrapolated from the interior cell centers in both phases. In addition, the interface location is predefined and considered to be fixed. The velocity components are calculated from the momentum conservation equations at the outlet boundary in both phases. However, different approaches are taken into account for setting the pressure in the two phases. In general, the pressure is specified at the outlet boundary of an incompressible flow field. In this two-phase flow, however, the exact interface location at the outlet is unknown, and therefore, the implementation of pressure at the outlet of each of two (liquid and gas) phases is not possible.

According to the role of continuity equation in coupling pressure and velocity fields, the mass transfer across the interface appears as the pressure difference between two phases. This pressure difference prevents imposing an equal pressure value for two phases at the outlet section. Therefore, the outlet pressure is set in one phase and interpolated for the other one.

The location of interface at outlet boundary is extrapolated from the interior interface points. The no-slip velocity and zero normal pressure gradient conditions are imposed on the wall boundaries.

B. Interface Boundary Conditions

Regarding the grid arrangement adjacent to the interface line, pressure and two velocity components for each phase are the six unknowns at the interface. The necessary equations for the mentioned unknowns are derived from the kinematic, dynamic, velocity continuity, and pressure boundary conditions.

Kinematic Boundary Condition:

While the interface location is predicted in an incorrect position, the kinematic condition would not satisfy mass transfer across the interface. The kinematic condition for a zero-thickness of the interface and with no mass transfer at the interface is represented by:

$$[(\mathbf{v}-\mathbf{v}_b)\cdot\mathbf{n}]_{\text{if}}=0 \tag{18}$$

where subscript "if" represents the interface. This boundary condition implies that the normal velocity of flow and the moving interface are equal.

Dynamic Boundary Condition:

This condition implies that the forces on the interface from both phases are in balance (momentum conservation on the interface). This means that the normal forces on both sides of the interface are equal in value but opposite in directions, i.e.

$$[(\mathbf{n}\cdot\mathbf{T})_1\cdot\mathbf{n}+\sigma K]_{\text{if}}=-[(\mathbf{n}\cdot\mathbf{T})_2\cdot\mathbf{n}]_{\text{if}} \tag{19}$$

The tangential forces are in balance along the interface for two phases:

$$[(\mathbf{n}\cdot\mathbf{T})_1\cdot\mathbf{t}-\partial\sigma/\partial t]_{\text{if}}=[(\mathbf{n}\cdot\mathbf{T})_2\cdot\mathbf{t}]_{\text{if}} \tag{20}$$

Here, $\mathbf{n}$, $\mathbf{t}$, K, and σ are the normal unit vector, tangential unit vector, interface curvature radius, and the surface tension, respectively. The subscripts 1 and 2 represent the phases 1 and 2, respectively. In the present work where the interface curvature is small, the surface tension terms are assumed to be negligible.

V. Interface Movement

For interface movement, the kinematic condition is used in accordance with the method proposed by Muzaferija and Peric [28]. The mass flow rate calculated from Lagrangian term is equal to the interface swept volume, and therefore, the mass flow across interface is derived from:

$$\dot{m}_{\text{if}}=\int_S[\rho(\mathbf{v}-\mathbf{v}_b)\cdot\mathbf{n}dS]_{\text{if}}=\rho\mathbf{v}_{if}\cdot\mathbf{n}S_{if}-\rho\mathbf{v}_{b,if}\cdot\mathbf{n}S_{\text{if}}=\rho\mathbf{v}_{\text{if}}\cdot\mathbf{n}S_{\text{if}}-\rho\dot{V}_{b,\text{if}} \tag{21}$$

If $\dot{m}_{\text{if}}$ is not zero, the surface should be displaced in a manner that the swept volume, $\dot{V}_{b,\text{if}}$, compensates this difference:

$$\dot{m}_{if}+\rho\dot{V}'_{b,\text{if}}=0 \tag{22}$$

On the other side, the swept volume can be defined by selecting the surface displacement direction as:

$$\dot{V}'_{b,\text{if}}=\frac{\Delta h}{\Delta t}S_{b,\text{if}}\mathbf{n}_{\text{if}}\cdot\mathbf{e}_{\text{if}} \tag{23}$$

Subsequently, the surface displacement Δh is obtained as:

$$\Delta h=\frac{\dot{V}'_{b,\text{if}}\Delta t}{S_{b,\text{if}}\mathbf{n}_{\text{if}}\cdot\mathbf{e}_{\text{if}}} \tag{24}$$

In the present problem, the $\mathbf{e}_{\text{if}}$ vector is assumed in normal direction to the channel wall. Fig. 5 shows the parameters of (24) adjacent to the interface.

The grid arrangement and nomenclature on both sides of the interface is shown in Fig. 5. The interface of two phases is considered to be represented as two adjacent cells with zero thickness. The centers of interface cells are located at the same place for two phases. In this way, the dynamic boundary conditions (balance of normal and tangential forces on the

interface) associates two cells at the interface and their neighbors. Accordingly, the discretized dynamic and kinematic equations at interface are added to the system of linear equations resulting from discretization of the two-phase flow field equations. The interface equations play the role of linking equations between the two phases and couple the two flow fields. This is an effective approach to maintain the implicitness and coupled nature of the numerical algorithm in this study. To the authors' knowledge, this approach has not been reported in previous similar studies.

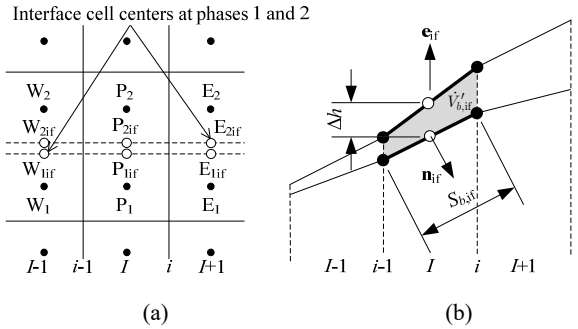

Fig. 5 Domain discretization at interface boundary; (a) boundary cells of phases 1 and 2, (b) grid point displacement parameters

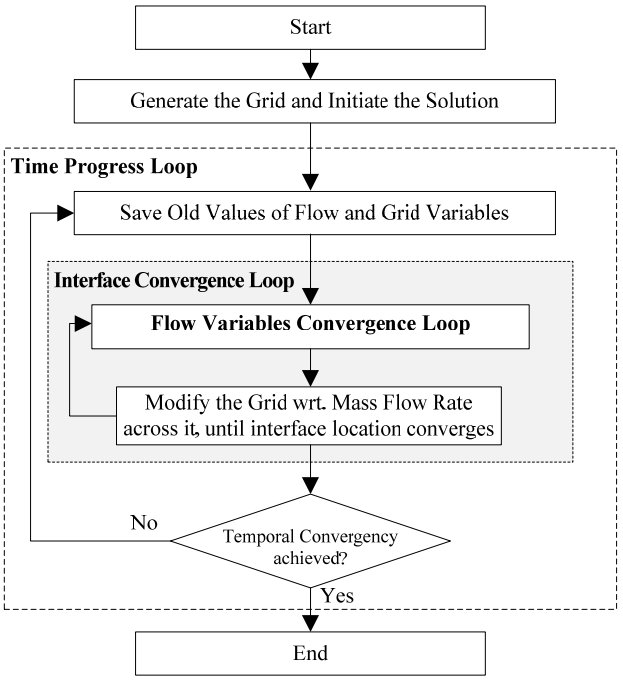

Fig. 6 Numerical solution algorithm for interface tracking

A. The Grid Structure and Displacement

In the present study, the interface front is tracked by the interface cell during an unsteady solving process. Therefore, the displacement of the internal grid points is proportional to the location of the interface at each time level. There are three general ways to displace the internal grid points [29]. The first is the algebraic method that moves each point of the grid using an algebraic function of one or several points on the interface. This method is very fast and simple, and is best used for structured grids on a relatively simple geometry with low distortions along the interface. The second is the elastic approach that assumes the grid structure as an elastic volume that obeys an imaginary correlation. Based on this correlation, a boundary value problem with known boundaries is defined and solved to obtain the location of the points inside the grid. This method is commonly used in rather complex geometries with an unstructured grid. The third is the regenerating the grid using the new location of the boundary points and adapting the old results on it. This method is suited for complex geometries with free boundaries, sharp curvatures, and intensive distortions.

In accordance with the simple geometry of two-phase flow inside a 2D channel, a non-orthogonal structured grid with an algebraic method of grid modification is used in this study. In this approach, the displacement of the interface points takes place only in the *y*-direction, and hence, the *x*-component of the points remains unchanged. Fig. 6 illustrates the current unsteady numerical algorithm developed for the unsteady interface tracking.

VI. Results and Discussion

A. Flow Field and Computational Grid

The flow field includes two zones related to each phase and is discretized by structured quadrilaterals. The channel height, H, is equal to unity, and its length is L=30H to50H. The first 5% of the channel length is assumed as the entrance length of the two phases. In entrance region, the interface height is fixed and considered as a no-slip wall boundary. This provides a reasonable velocity gradient at the section where the interface starts to develop. Fig. 7 shows the grid structure at the solution onset with an assumption that the interface is initially located at y=0.3H. During the solution process, the grid changes to reach a steady state condition according to the interface boundary condition.

To study the grid dependency of the numerical solution, the most sensitive two-phase flow field is studied where the viscosity, density, and volumetric flow rate ratios are 50, 1000, and 0.01, respectively. In this case, the gravitational force is assumed to be zero. Since the flow variations in x direction are small, a uniformly distributed grid with 100 cells is used in the x-direction. However, in the y-direction, there are considerable changes in velocity and shear stresses and hence, evaluation of the grid size in this direction is needed. The cell numbers in the y-direction were increased from 10 to 40 cells (5 to 20 cells for each phase) with uniform distribution. Then, the total relative error of interface location and maximum velocity was computed using the following general formulation:

$$Error(\%) = \frac{\varphi_{Num} - \varphi_{AS}}{\varphi_{AS}} \times 100 \qquad (25)$$

where, φ_{Num} and φ_{AS} are extracted from numerical and analytical solutions and *Error* is the total relative error percent. As shown in Fig. 8, there would be a reasonable

decrease in numerical solution error by increasing cell numbers up to 30. The accuracy of numerical solution does not experience a significant change for the grid with cell numbers above 30 along the *y* direction. In this situation, the error of the interface location and maximum velocity are lower than 1%. Therefore, a grid with 100 cells in *x*-direction and 30 cells in *y*-direction is utilized for computations carried out in this study.

B. Two-Phase Flow in Zero Gravitational Force

As described in analytical solution section, the two-phase flow is independent of density ratio at zero gravitational force. Thus, in this section, only the effects of volumetric flow rate ratio and viscosity ratio are considered. Six different cases based on the combinations of two volumetric flow rate ratios of 0.1 and 0.01 and three viscosity ratios of 1, 10, and 50 were simulated. The flow with viscosity ratio of 50 is similar to the case of water and steam flow. For each case, temporal changes of the interface location are presented, and the fully developed velocity profile and interface location are compared with those of analytical solutions.

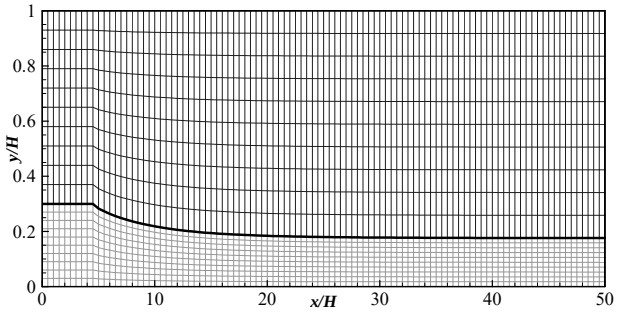

Fig. 7 Grid generated for two-phase flow with an interface initially at $y = 0.3H$

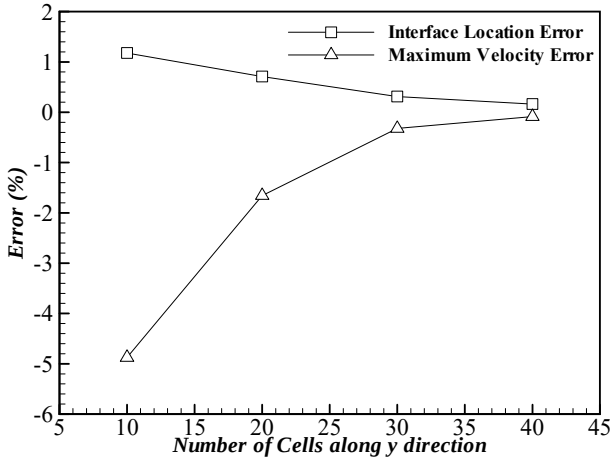

Fig. 8 The effect of number of grid cells along *y* direction on numerical solution accuracy at viscosity ratio of 50, density ration of 1000, Re to Fr number of zero, and volume rate of 0.01

1) Interface Location and Velocity Profile

The first flow cases are those at volumetric flow rate of 0.1 which are tested in three viscosity ratios of 1, 10 and 50. Temporal changes of the interface location for these three cases are shown in Fig. 9 (a). As expected from (12), the two-phase flow at zero gravitational force depends only to the viscosity and the volumetric flow rate ratios. Hence, according to the results given in Fig. 10 (a), at viscosity ratio of 1 (two similar fluids), the fully developed location of interface is calculated to be in a place where the velocity gradients are equal in both sides of interface.

The increase in viscosity ratio causes the interface location to rise. This rise occurs because of the balance of shear forces of the two phases at the interface. That is, in accordance to (6), the higher viscosity fluid reaches to shear force balance in a lower velocity gradient, and vice versa. This trend can be seen in Fig. 10 (a) showing the velocity profile and interface location changes due to increase in dynamic viscosity ratio. In this figure, the comparison between the analytical and numerical results shows good agreement.

Decrease of volumetric flow rate ratio from 0.1 to 0.01, results in lower flow film thickness of phase 1. The film thickness is estimated to be placed at a lower value than 0.06 for viscosity ratio of 1. Increase in the viscosity ratio, similar to the previous conditions, leads to a higher film thickness of phase 1 (see Figs. 9 (b) and 10 (b)).

2) Time Variations of Interface Location to Reach Steady State

The temporal variations of interface location are illustrated in Fig. 9. Firstly, the higher viscosity ratio generates the interface with higher frequency, and its amplitude increases with time. For instance, for a volumetric flow rate of 0.1, increasing the viscosity ratio from 1 to 10 and then to 50 leads to an increase in interface fluctuations from about 10% to 120% and 400%, respectively. Secondly, as the viscosity ratio decreases, the flow field reaches to the fully developed condition in a shorter length of channel. For example, in volumetric flow rate and viscosity ratios of one, the steady-state condition occurs by a length of 3H. For viscosity ratios of 10 and 50, the development length increases up to about 15*H* and 40*H*, respectively. Similar observations for volumetric flow rate ratios of 0.1 and 0.01 can be seen in the plots of Fig. 9. Moreover, the effect of increase in fluctuations on the flow field is considerable. If the channel length is considered 100H instead of 50H, the continuous increase of fluctuations amplitude may lead to collision with upper wall and blockage of the channel to phase 2.

TABLE I
COMPARISON BETWEEN NUMERICAL AND ANALYTICAL SOLUTIONS FOR INTERFACE LOCATION (*F*) IN ABSENCE OF GRAVITY

Case	f_Q	f_μ	Re_1/Fr_1	f_{AS}	f_{Num}	Error
1	0.1	1	0	0.18599	0.18691	0.49%
2	0.1	10	0	0.33488	0.33643	0.46%
3	0.1	50	0	0.47831	0.48041	0.44%
4	0.01	1	0	0.05861	0.05909	0.83%
5	0.01	10	0	0.14598	0.14703	0.72%
6	0.01	50	0	0.25582	0.25762	0.70%

3) Numerical Solution Error Evaluation

The comparison of numerical and analytical results regarding the interface location for the mentioned six cases (flow in zero gravitational force) is denoted in Table I. The interface location is shown as f_{AS} for analytical and f_{NUM} for numerical solutions. It is observed from this table that the error is 0.83% or less. Two observations were made regarding these results. First, there is a gradual increase in error with a decrease in volumetric flow rate ratio (f_Q). This trend is related to the interface profile. The interface profile experiences more curvature in lower f_Q until reaching a completely developed state. Therefore, extending the channel length results in a more developed flow lowers numerical error. Second, the error increases with increasing viscosity ratio. This trend also comes from an interface profile that takes longer to reach the converged state.

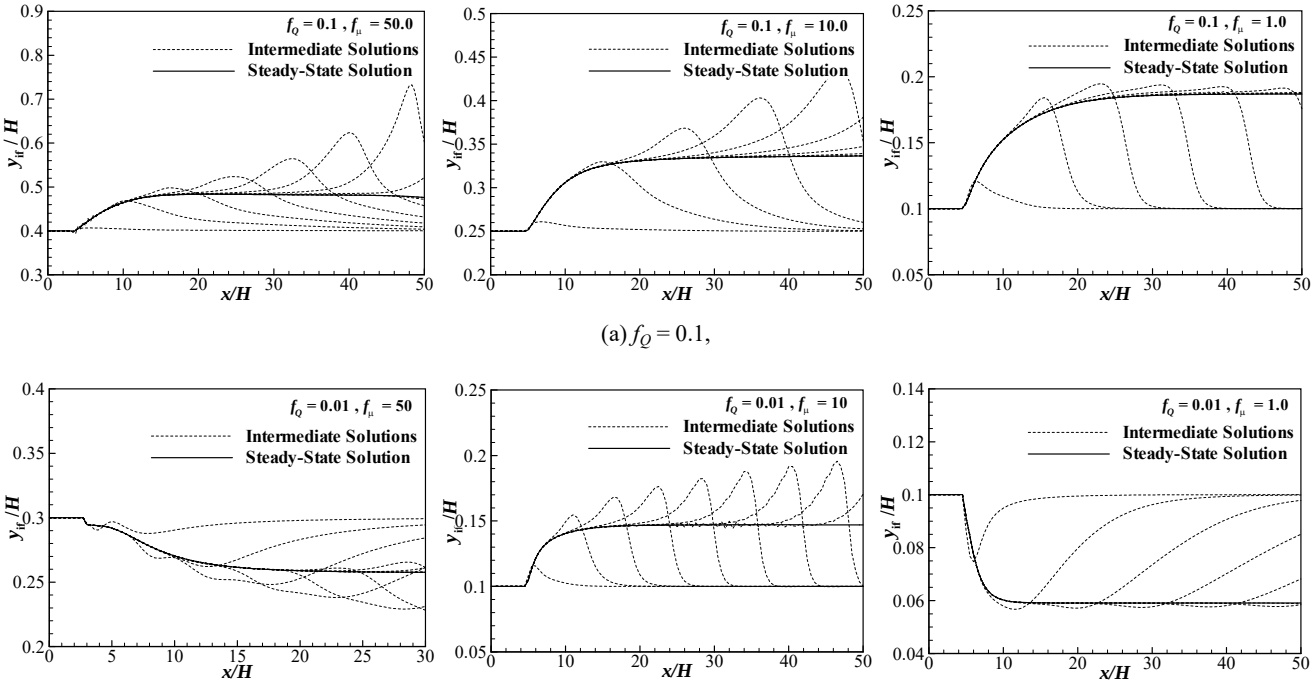

(a) $f_Q = 0.1$,

(b) $f_Q = 0.01$,

Fig. 9 Intermediate and steady-state solutions for interface profile

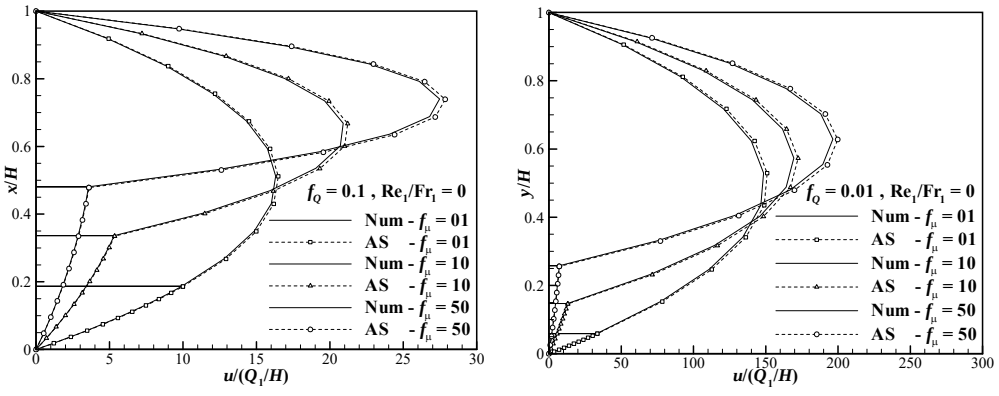

(a) $f_Q = 0.1$ (b) $f_Q = 0.01$

Fig. 10 Comparison of analytical and numerical solutions at zero gravitational force and f_μ = 1, 10, and 50

C. Effects of Gravitational Force on Two-Phase Flow

The effects of viscosity and volumetric flow rate ratio are investigated in detail in previous section. Similar numerical results were carried out for a flow field under a gravitational force. From (11b) and (13d), the interface location is almost independent of the density ratio at large density ratios (f_ρ>>1). Therefore, only the effects of volumetric flow rate and Reynolds-to-Froude number ratios are considered in this section. To create more realistic conditions for the two-phase flows of water and steam, viscosity and density ratios are set to 1000 and 50, respectively. Six cases were established considering volumetric flow rate ratios of 0.1 and 0.01 and

Reynolds-to-Froude number ratios of -2, 0, and +2. Favorable Froude number stands for the case that the gravitational force (acceleration) is in direction of the flow and adverse one stands for the case that gravitational force is in opposite direction of the flow. It is worth noting that, for these flow conditions, the Re_1/Fr_1 = +2 is equivalent, for example, to a channel height of 2mm with inclination angles of 5.5º and 28º for volumetric flow rate ratios of 0.1, and 0.01, respectively. Also, for Fr_1/Re_1 = -2, the inclination angles will be -2.0º, and -5.5º for volumetric flow rate ratios of 0.1 and 0.01, respectively (see Fig. 11).

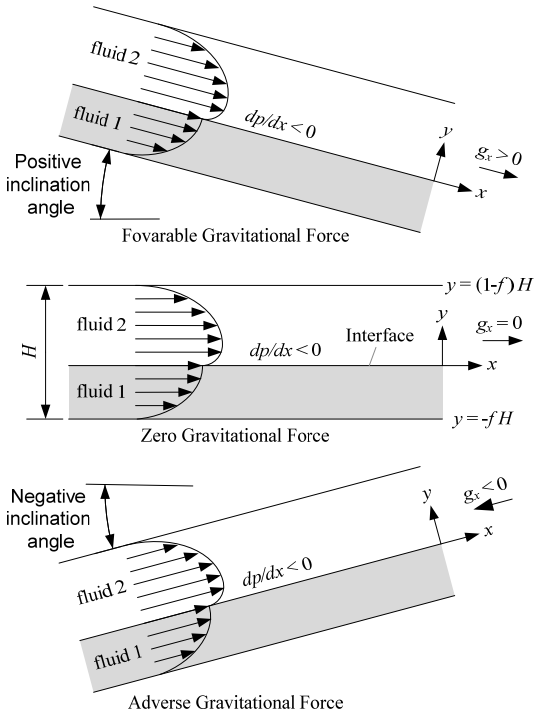

Fig. 11 Schematic two-phase channel flow with favorable pressure gradient and favorable, zero, and adverse gravitational force

Implementing favorable gravitational force in two-phase flow results in velocity increase for the fluid with higher density. This leads to a lower thickness of film flow of fluid with higher density. Fig. 12 depicts the effect of gravitational force in three volumetric flow rate ratios of 0.1 and 0.01. As is seen in this figure, in favorable gravitational force (Re_1/Fr_1=+2), the thickness of phase 1 decreases compared to the zero gravitational force (Re_1/Fr_1=0) case. This reduction is about 21% and 31% for volumetric flow rate ratios of 0.1, and 0.01, respectively.

In adverse gravitational force (Re_1/Fr_1=-2), the phase 1 film thickness increases about 10% and 17% for volumetric flow rate ratios of 0.1 and 0.01, respectively. The comparisons between the favorable and adverse gravitational forces show that the variations of interface location for favorable gravitational force is about 2 times more than its variations in adverse state. These results are compared in Table II.

In Table II, the numerical and analytical results are summarized for flow under a gravitational force. The interface locations obtained from analytical and numerical solutions are shown as f_{AS} and f_{NUM}, respectively. It is seen that the error level is mostly below 1%.

TABLE II
COMPARISON BETWEEN THE NUMERICAL AND ANALYTICAL SOLUTIONS FOR INTERFACE LOCATION

Case	f_Q	Re_1/Fr_1	f_{AS}	f_{Num}	Error	Change wrt. zero gravitational force
1	0.1	2-	0.52629	0.52954	0.62%	10.03%
2	0.1	0	0.47831	0.48041	0.44%	0.00%
3	0.1	2	0.37668	0.37925	0.68%	21.25%-
4	0.01	2-	0.29916	0.3007	0.52%	16.94%
5	0.01	0	0.25582	0.25762	0.70%	0.00%
6	0.01	2	0.17585	0.17616	0.18%	31.26%-

* For all cases, f_μ = 50 and f_ρ = 1000.

VII. CONCLUSION

In a gas-liquid two-phase flow, fluid thermophysical properties can be significantly different at the interface of the two phases. One of the most challenging parts of the numerical simulation of these types of flow is to determine the location of the interface accurately. In the present work, a coupled interface tracking algorithm was developed based on ALE approach using a cell-centered pressure-based finite volume method. Firstly, the analytical solution of the flow problem without a gravitational force was obtained within a 2D channel. Secondly, in order to verify present coupled algorithm, the results of numerical simulations were compared with those of analytical solution at various flow conditions. The variation of the interface location versus various non-dimensional parameters such as the ratio of volumetric flow rate of two fluids, their dynamic viscosity ratio, their density ratio and the ratio of Reynolds-to-Froude numbers was studied. The analytical results showed that the interface location is independent of the density ratio of two fluids in zero gravity condition. In addition, for very high values of density ratio, the effect of variation of density ratio on the interface location reduces considerably. The evaluation of the developed numerical algorithm, regarding the process of interface tracking, was accomplished assuming two cases of zero gravity condition and the case with consideration of gravity effects.

Although a relatively coarse and uniform grid was employed in the simulations, the numerical results show a good accuracy compared with the results of analytical solution. Temporal variations of interface profile toward reaching to the steady-state condition showed that increment of the difference between the properties of two fluids (especially their dynamic viscosity) will result in generation of larger traveling waves in their interface. Moreover, at steady-state conditions, the interface profile of two fluids with different viscosity and flow rate ratios requires further length in flow direction to reach to its final equilibrium location. Examination of velocity profile indicates that the employed numerical algorithm has been able to adapt with the variation of viscosity ratio, which is a significant parameter for

determination of the interface location. The developed modeling approach enforces an accurate balance of shear forces at the phase interface. The study of the gravity effect showed that favorable gravity (gravity in direction of the flow) will result in reduction of the thickness of heavier fluid compared to zero gravity, as expected. In contrast, the adverse gravity (gravity in opposite direction of the flow) would lead to increment of the heavier fluid thickness compared with the case of zero gravity condition. However, it is worth noting that the amount of variation in favorable gravity is much more than the case of adverse gravity.

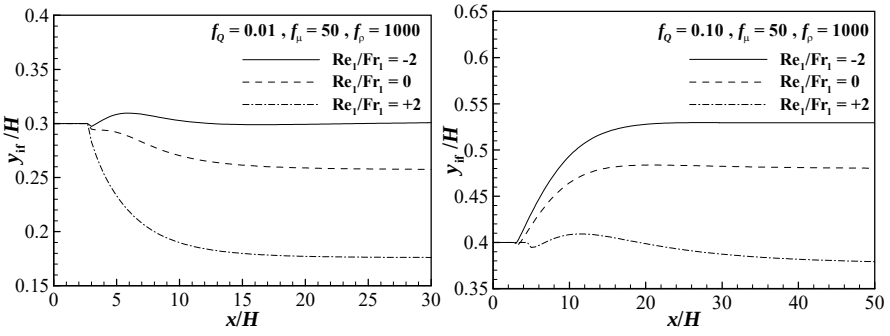

(a) steady-state interface profiles

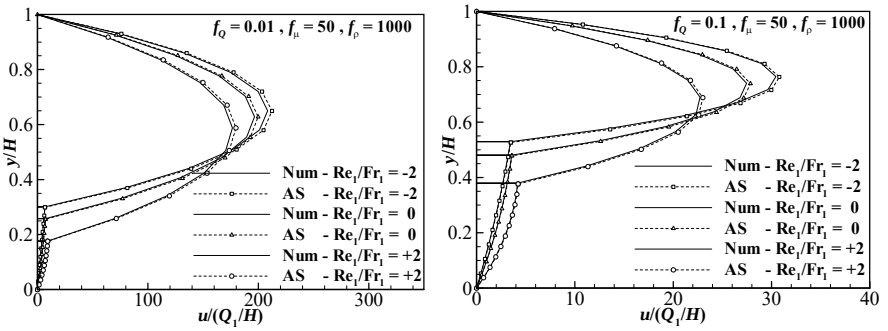

(b) velocity profiles

Fig. 12 Interface location and velocity profile versus Re_1/Fr_1 at f_μ = 50 and f_ρ = 1000

REFERENCES

[1] J. Weisman, "Two-phase flow patterns," in Handbook of Fluids in Motion, N. P. Cheremisinoff and R. Gupta, Ed. Ann Arbor Science Publication, 1983, pp. 409-425.

[2] J. H. Ferziger and M. Peric, Computational methods for fluid dynamics. Springer Science & Business Media, 2012.

[3] J. M. Floryan and H. Rasmussen, "Numerical methods for viscous flows with moving boundaries," Appl. Mech. Rev., vol. 42, no. 12, pp. 323-341, 1989.

[4] F. H. Harlow and J. E. Welch, "Numerical calculation of time-dependent viscous incompressible flow of fluid with free surface," Phys. Fluids, vol. 8, no. 12, p. 2182, 1965.

[5] C. W. Hirt and B. D. Nichols, "Volume of fluid (VOF) method for the dynamics of free boundaries," J. Comput. Phys. vol. 39, no. 1, pp. 201-225, 1981.

[6] J. U. Brackbill, D. B. Kothe, and C. Zemach, "A Continuum Method for Modeling Surface Tension," J. Comput. Phys., vol. 100, no. 2, pp. 335-354, 1992.

[7] S. Chen, D. B. Johnson, P. E. Raad, and D. Fadda, "The surface marker and micro cell method," Int. J. Numer. Meth. Fl., vol. 25, no. 7, pp. 749-778, 1997.

[8] M. Sussman, P. Smereka, and S. Osher, "A Level Set Approach for Computing Solutions to Incompressible Two-Phase Flows," J. Comput. Phys., vol. 114, no. 1, pp. 146-159, 1994.

[9] S. Osher and R. P. Fedkiw, "Level Set Methods," J. Comput. Phys., vol. 169, no. 2, pp. 463-502, 2001.

[10] J. A. Sethian, "Evolution, Implementation, and Application of Level Set and Fast Marching Methods for Advancing Fronts," J. Comput. Phys., vol. 169, no. 2, pp. 503-555, 2001.

[11] G. D. Raithby, W. X. Xu, and G. D. Stubley, "Prediction of incompressible free surface with an element-based finite volume method," J. Comput. Fl. Dyn., vol. 4, no. 3, pp. 353-371, 1995.

[12] Demirdzic and M. Peric, "Finite volume method for prediction of fluid flow in arbitrarily shaped domains with moving boundaries," Int. J. Numer. Meth. Fl., vol. 10, no. 7, pp. 771-790, 1990.

[13] E. S. Oran and J. P. Boris, Numerical Simulation of Reactive Flow, Elsevier, New York, 1987.

[14] P. J. Shopov, P. D. Minev, I. B. Bazhekov, and Z. D. Zapryanov, "Interaction of a Deformable Bubble with a Rigid Wall at Moderate Reynolds Numbers," J. Fluid Mech., vol. 219, pp. 241-271, 1990.

[15] J. Feng, H. H. Hu, and D. D. Joseph, "Direct Simulation of Initial Value Problems for the Motion of Solid Bodies in a Newtonian Fluid, Part 1. Sedimentation," J. Fluid Mech., vol. 261, pp. 95-134, 1994.

[16] J. Feng, H. H. Hu, and D. D. Joseph, "Direct Simulation of Initial Value Problems for the Motion of Solid Bodies in a Newtonian Fluid, Part 2. Couette and Poiseuille Flows," J. Fluid Mech., vol. 277, pp. 271-301, 1995.

[17] H. H. Hu, "Direct Simulation of Flows of Solid-Liquid Mixtures," Int. J. Multiphase Flow, vol. 22, no. 2, pp. 335-352, 1996.

[18] J. Fukai, Y. Shiiba, T. Yamamoto, O. Miyatake, D. Poulikakos, C. M. Megaridis, and Z. Zhao, "Wetting Effects on the Spreading of a Liquid Droplet Colliding with a Flat Surface: Experiment and Modeling," Phys. Fluids, vol. 7, no. 2, pp. 236-247, 1995.

[19] J. Glimm, J. W. Grove, X. L. Li, W. Oh, and D. H. Sharp, "A critical analysis of Rayleigh-Taylor growth rates," J. Comput. Phys., vol. 169, no. 2, pp. 652-677, 2001.

[20] S. O. Unverdi and G. Tryggvason, "A Front-Tracking Method for Viscous, Incompressible, Multi-Fluid Flows," J. Comput. Phys., vol. 100, no. 1, pp. 25-37, 1992.

[21] G. Tryggvason, B. Bunner, A. Esmaeeli, D. Juric, N. Al-Rawahi, W. Tauber, J. Han, S. Nas, and Y-J. Jan, "A front-tracking method for the computations of multiphase flow," J. Comput. Phys., vol. 169, no. 2, pp. 708-759, 2001.
[22] F. Hassaninejadafarahani and S. Ormiston, "Numerical Analysis of Laminar Reflux Condensation from Gas-Vapour Mixtures in Vertical Parallel Plate Channels," World Academy of Science, Engineering and Technology, Int. J. Mech., Aer., Ind., Mech. and Manuf. Eng., vol. 9, no. 5, pp. 778-785, 2015.
[23] M. A. Islam, A. Miyara, T. Nosoko, and T. Setoguchi, "Numerical investigation of kinetic energy and surface energy of wavy falling liquid film," J. Therm. Sci., vol. 16, no. 3, 237-242, 2007.
[24] R. W. Fox and T. A. McDonald, Introduction to fluid mechanics, John Wiley, 1994.
[25] Demirdzic and M. Peric, "Space conservation law in finite volume calculations of fluid flow," Int. J. Numer. Meth. Fl., vol. 8, no. 9, pp. 1037-1050, 1988.
[26] C. M. Rhie and W. L. Chow, "Numerical Study of the Turbulent Flow Past an Airfoil with Trailing Edge Separation," AIAA Journal, vol. 21, no. 11, pp. 1525–1532, 1983.
[27] S. Vakilipour and S. J. Ormiston, "A coupled pressure-based co-located finite-volume solution method for natural-convection flows," Numer. Heat Tr., B-Fund., vol. 61, no. 2, pp. 91-115, 2012.
[28] S. Muzaferija and M. Peric, "Computation of free-surface flows using the finite-volume method and moving grids," Numer. Heat Transfer, vol. 32, no. 4, pp. 369-384, 1997.
[29] T. E. Tezduyar, S. Aliabadi, M. Behr, A. Johnson, V. Kalro, and M. Litke, "Flow simulation and high performance computing," Comput. Mech., vol. 18, no. 6, pp. 397–412, 1996.